MODELLING GEOMETRY OF SPACEBORNE CCD LINEAR ARRAY SENSOR-EXPERIENCES WITH JERS/VNIR IMAGES

Xiaowei Yu, Eija Honkavaara, Juha Jaakkola and Janne Ylönen
Finnish Geodetic Institute
Finland
Geodeetinrinne 2, 02430 Masala

ABSTRACT

As part of the multisensor aerial triangulation system, mathematical models for describing the imaging geometry of spaceborne CCD linear array sensor were presented and evaluated for use in the orientation process. The satellite orbit is modelled using a set of four parameters and variations of the satellite attitude with time are modelled using second-order polynomials. The image space and object space are related by collinearity equations. The unknown parameters are solved by using least-squares technique. The parameters thus derived can serve as the basis for geometrical correction, DTM generation, ortho-image production and so on. The evaluations were made using JERS images for 1) single image, 2) a strip of three images and 3) stereopair. The preliminary results show that an accuracy of about 0.4 pixels both in X and Y could be achieved using nine control points without attitude information. RMSEs of 10.7m in X, 7.2m in Y and 17.9m in Z were obtained for a stereopair when four control points were used.

1. INTRODUCTION

The geometry of satellite imageries based on the "push broom" principle differs significantly from that photogrammetric frame camera because their instantaneous optical imaging is restricted to a single plane containing the CCD linear array sensor (Kratky, 1989). Since the position and attitude of CCD linear array sensor are continuously changing along the orbit, the imaging geometry thus becomes dynamic and time-dependent (Fig 1).

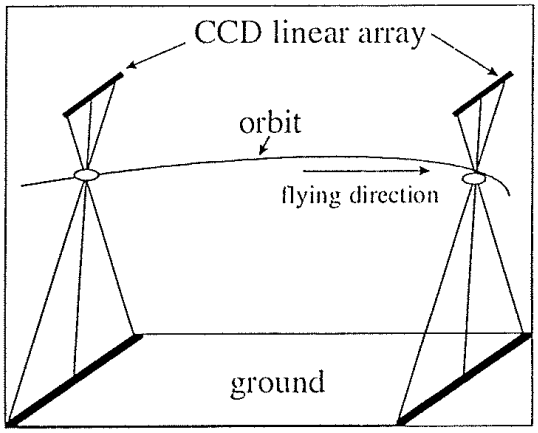

Figure 1. Imaging geometry of CCD linear array sensor.

Examples of satellite sensors with the CCD linear array sensor geometry are SPOT/HRV, which is very well known and widely used; MOMS/Pan, which is equipped with three CCD linear array sensors looking at nadir, forward and backward respectively; IRS/Pan, which uses three CCD linear arrays in imaging of a single line and JERS/VNIR. Furthermore, many of the future optical high resolution satellite will equipped with the CCD linear array sensor, for instance, QuickBird/Pan, Orbview/Pan and IKONOS.

Mathematical models for describing the geometry of imageries acquired by CCD linear array sensors have be developed during past years (Neto, 1988; Kratky, 1988; Westin, 1990, 1991; Ebner *et. al.* 1992; Maruyama *et. al.*, 1994; Jacobsen, 1997). These methods combine satellite orbit and/or attitude observations and ground control points (GCPs) to obtain geometric solutions. However, they differ in the modelling of orbit and attitude of satellite.

This study is based on the Westin's approach for modelling the geometry of satellite CCD linear array sensors. The model has been successfully used with SPOT/HRV and JERS/VNIR images (Westin, 1990, 1991 and 1996). Some modifications have been made to make the approach more general. For instance, second order polynomials are used to model the attitude variations.

In the following we first present the geometry of JERS images, and then describe models for position and attitude of CCD linear array sensor. Finally empirical test set up is described and empirical results are given.

2. GEOMETRY AND CHARACTERISTICS OF JERS IMAGES

JERS is a sun-synchronous near circular orbiting satellite launched by Japan in 1992. Satellite carries two instruments (OPS and SAR). OPS/VNIR sensor records images, which cover 75 km x 75 km areas in four channels, at altitude of 568km. Channels 1-3 are looking at nadir and channel 4, which has the same spectral sensitivity as channel 3, is looking 15.33° forward. This gives the possibility of along track stereo images with B/H=0.3 (Fig 2). The pixel size is about 24 m along track and 18 m across track. JERS images are not received anymore.

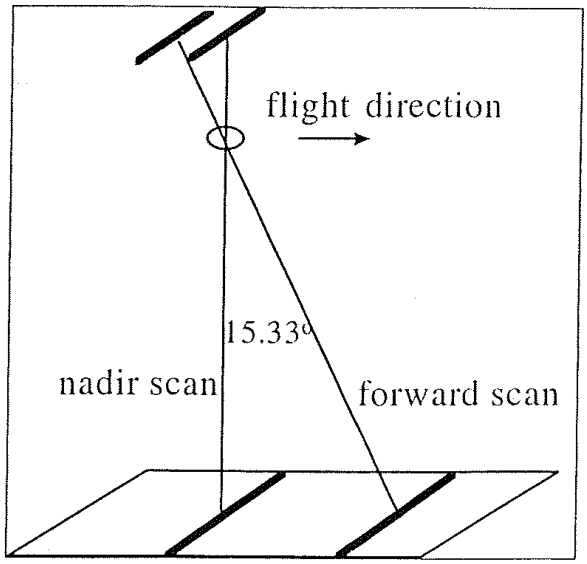

Figure 2. Imaging Geometry of JERS/VNIR sensor.

Photogrammetric quality of the JERS VNIR images is not high, because of poor resolution and small B/H-ratio. However, VNIR images were selected to be the empirical test material, since it was the only available satellite sensor producing along track stereo data of Finland.

3. MATHEMATICAL MODELS

Photogrammetric solution of JERS image geometry through block adjustment comprises the determination of ground coordinates of measured points and orientation of the satellite sensor, i.e. the position and attitude of the sensor. Since each line of image is captured by CCD linear array sensor at different time, each line has its own orientation parameters. It is neither possible nor necessary to determine the orientation parameters of all image lines, because not only are these parameters too many, but also they are

highly correlated. As a consequence of this, the satellite position and attitude changes are modelled mathematically.

3.1 Orbital Model

Satellite orbit and its position in the orbit can be determined by six orbital elements according to Kepler's law. One set of these elements is: semi-major axis (a) and eccentricity (e), which define the size and shape of the orbit; right ascension of ascending node (Ω), inclination (i) and argument of perigee (ϖ), which define the orientation of the orbit; and true anomaly (v), which gives the satellite position in the orbit (Fig 3). Due to the disturbing noncentral forces, mainly second-degree zonal component of the earth gravitational potential, satellite orbit deviates from the elliptic form (Westin, 1990).

It has been proved that satellite orbit can be approximated by a circular orbit with sufficient accuracy during the pass of one scene (Westin, 1990). The orbit radius is however allowed to vary with time to account for the elliptic from. The radial shape of the orbit is determined by fitting a third-order polynomial in time to the orbital radii derived from the ephemeris. This shape is considered fixed except the constant term. Thus the orbital elements needed to be estimated can be reduced to four: inclination (i), right ascension of ascending node (Ω), time at ascending node (t_0) and orbital radius at the ascending node (r_0) (Westin, 1990). The initial values of four orbital parameters can be derived from ephemeris data provided by fitting them to first-order (i, Ω, t_0) and third-order (r_0) polynomials.

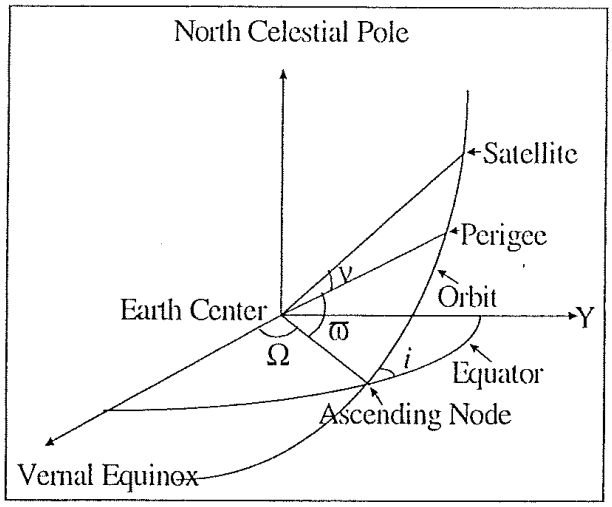

Figure 3. Satellite orbit and orbital parameters.

3.2 Attitude Model

In addition to the satellite orbit and position, the sensor attitude has to be determined too. In this study, second-order polynomials have been used to model the time dependent variations of sensor attitude as given by

$$\begin{aligned} w(t) &= w_0 + w_1 t + w_2 t^2 \quad \text{for roll angle} \\ \rho(t) &= \rho_0 + \rho_1 t + \rho_2 t^2 \quad \text{for pitch angle} \\ \kappa(t) &= \kappa_0 + \kappa_1 t + \kappa_2 t^2 \quad \text{for yaw angle} \end{aligned} \tag{1}$$

It is not necessary to use all the terms in the adjustment. For instance, Westin has assumed that the angle observations are of sufficient accurate, and treated only the constant offset terms as unknowns (Westin 1990, Westin 1996). Experiments have shown that linear and quadratic terms are sometimes necessary, because of possible bias in the angle rate measurements (Priebbenow, 1992, Nwosu and Meid, 1996).

3.3 Imaging Geometry

The image to ground coordinate relationship is established through the collinearity equations:

$$0 = -f \frac{m_{11}(X - X_s) + m_{12}(Y - Y_s) + m_{13}(Z - Z_s)}{m_{31}(X - X_s) + m_{32}(Y - Y_s) + m_{33}(Z - Z_s)} \tag{2}$$

$$y = -f \frac{m_{21}(X - X_s) + m_{22}(Y - Y_s) + m_{23}(Z - Z_s)}{m_{31}(X - X_s) + m_{32}(Y - Y_s) + m_{33}(Z - Z_s)}. \tag{3}$$

In matrix form this becomes:

$$\begin{bmatrix} 0 \\ y \\ -f \end{bmatrix} = \frac{1}{d} \begin{bmatrix} m_{11} & m_{12} & m_{13} \\ m_{21} & m_{22} & m_{23} \\ m_{31} & m_{32} & m_{33} \end{bmatrix} \begin{bmatrix} X - X_s \\ Y - Y_s \\ Z - Z_s \end{bmatrix} = \frac{1}{d} M \begin{bmatrix} X - X_s \\ Y - Y_s \\ Z - Z_s \end{bmatrix}, \tag{4}$$

where $[0, y, f]^T$ are the image coordinates in *sensor coordinate system*, d is the scaling factor, $[X_s, Y_s, Z_s]^T$ are the coordinates of satellite in the *earth centered inertial coordinate system* (ECI), $[X, Y, Z]^T$ are the coordinates of ground points in ECI and M is the orthogonal rotation matrix to make the transformation from ECI to the sensor coordinate system.

The sensor coordinate system has the origin at the perspective centre, the y-axis is parallel to the array of CCD line, the z-axis is perpendicular to the y-axis and x-axis completes a right-handed system. As the CCD linear array is one-dimensional, the x-coordinate is always zero in the sensor coordinate system and x-coordinate observations are converted to time at which image data are acquired.

The transformation from the geodetic coordinate system, in which control information are normally given, to the sensor coordinate system involves a series of transformations, see Fig 4. The input to the system is the coordinates in the earth centred earth fixed coordinate system (ECEF) like WGS84. The transformation of ground points from geodetic coordinate system to ECI can be performed in two steps: first coordinates are transformed to ECEF and then from ECEF to ECI by applying orthogonal rotation matrix R_e, which is the function of Greenwich hour angle.

The orthogonal transformation matrix, M, from ECI to the sensor coordinate system consists of three rotations and is expresses as:

$$M = (R_{IF} \cdot R_{FB} \cdot R_{BS})^T, \tag{5}$$

where R_{IF} is the flight-inertial transformation, R_{FB} is the body-flight transformation and R_{BS} is the sensor-body transformation.

R_{IF} relates the *orbital reference system* to the ECI. It is the function of orbital parameters and defined by

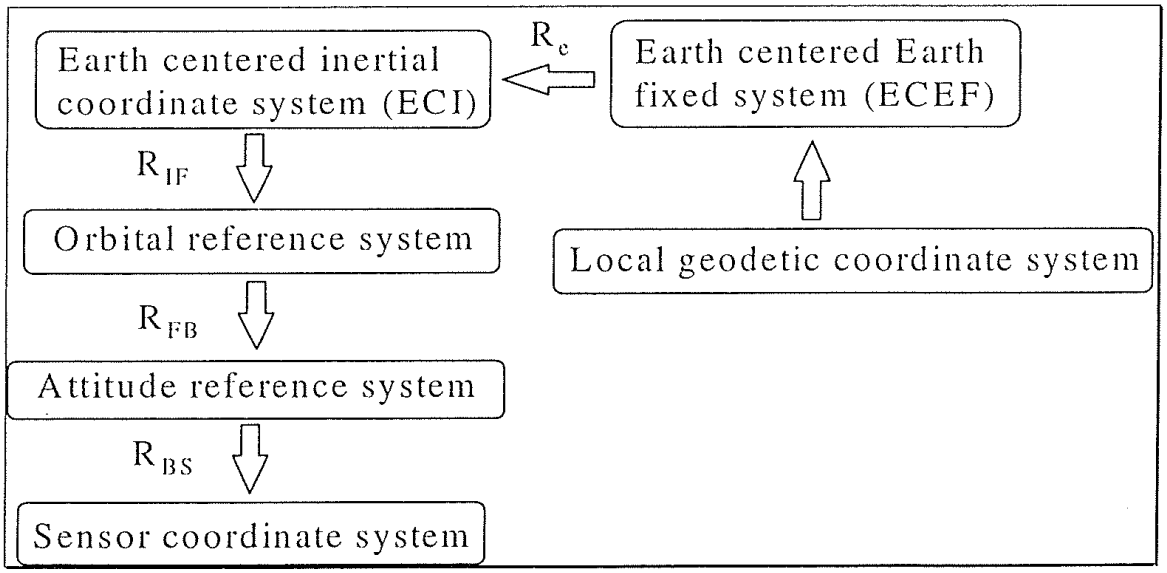

Figure 4. Coordinate systems and transformations.

$$R_{IF} = \begin{bmatrix} -\cos\Omega\sin u - \sin\Omega\cos i\cos u & \sin\Omega\sin i & \cos\Omega\cos u - \sin\Omega\cos i\sin u \\ -\sin\Omega\sin u + \cos\Omega\cos i\cos u & -\cos\Omega\sin i & \sin\Omega\cos u + \cos\Omega\cos i\sin u \\ \sin i\cos u & \cos i & \sin i\sin u \end{bmatrix}. \quad (6)$$

The central travel angle, u, is defined by

$$u = \varpi + v = (t - t_0)\frac{2\pi}{T}, \quad (7)$$

where T is the satellite period.

R_{FB} relates the *attitude reference system* to the orbital reference system. It is the function of attitude angles and defined by

$$R_{FB} = \begin{bmatrix} \cos\rho\cos\kappa & \sin\omega\sin\rho\cos\kappa + \cos\omega\sin\kappa & -\cos\omega\sin\rho\cos\kappa + \sin\omega\sin\kappa \\ -\cos\rho\sin\kappa & -\sin\omega\sin\rho\sin\kappa + \cos\omega\cos\kappa & \cos\omega\sin\rho\sin\kappa + \sin\omega\cos\kappa \\ \sin\rho & -\sin\omega\cos\rho & \cos\omega\cos\rho \end{bmatrix}. \quad (8)$$

R_{BS} relates the sensor coordinate system to the attitude reference system. It accounts for the viewing angle and alignment offsets of CCD linear array. It is thus constant within one scene for one particular sensor. The system can accommodate for the absence of this rotation in the model. Accordingly, the viewing angle can be used as an initial value for ω or ρ instead of zero value (Nwosu and Meid, 1996).

All the variables in the right hand side of equations (2) and (3) are the functions of time. For more details refer to Westin (1990 and 1991).

3.4 Adjustment

The satellite orientation can be determined by four orbital parameters and three to nine attitude parameters, thus in the case of single scene, the full set of unknown orientation parameters is the following [i, Ω, r_0, t_0, ω_0, ω_1, ω_2, ρ_0, ρ_1, ρ_2, κ_0, κ_1, κ_2].

The same model can be applied to multi-scene of one pass when unknown orientation parameters are regarded as the corrections to the different sets of initial values of orientation parameters for each scene (Westin, 1991). In this way, the orientation parameters are kept the same as processing single scene. Thus requirements for GCP are reduced greatly for each image. But in order to obtain a solution in the cases when there are gaps in the sequence of scenes, the orientation parameters are divided into two groups: strip parameters including [i, Ω, r_0], applying to the whole pass; and scene parameters including [t_0, ω, ρ, κ], which are different for each image (Westin 1991). This formulation allows orientation of single scene as well as of large blocks with several passes and along or across track stereo overlap.

The unknown orientation parameters can be solved by the well known photogrammetric block adjustment techniques. In the adjustment, the possible observations are ground coordinates of GCPs, image coordinates of GCPs and tie points, and orientation parameters. The unknowns are the orientation parameters as well as unknown ground coordinates. The observations of orientation parameters are important to stabilise the system in the case of poor ground control configuration in which system could become singular due to the high correlation between orientation parameters (Westin, 1990).

The non-linear observation equations are linearised by utilising the first order terms from the Taylor's series expansion. The final adjustment model is the following

$$AV + B\Delta = F\,, \tag{9}$$

where A is the matrix containing the first-order partial derivatives with respect to the observations, B is the matrix containing the first-order partial derivatives with respect to the orientation parameters, V is the vector of observation residuals, Δ is the vector of corrections, F is the collinearity equations with observations and approximated parameter values. For more details refer to (Mikhail, 1976, Westin, 1991).

The solution can be obtained by the iterative weighted least-squares. The improvements in each iteration round are (Mikhail, 1976, Westin, 1991):

$$\Delta = (B^T(AQA^T)^{-1}B)^{-1}B^T(AQA^T)^{-1}F\,, \tag{10}$$

where Q is the cofactor matrix for the observations.

The model for JERS VNIR images has now been implemented into the multisensor aerial triangulation system being under development at Finnish Geodetic Institute (FGI).

4. TEST AREA AND MATERIALS

Empirical investigations were made using JERS images acquired at 25 of June, 1995 during one orbit pass. The strip of images consists of five images, which cover an area of about 75km x 375km from middle to southern Finland. However, only three adjacent

images were used because of geometric errors in other two images (missing lines). Data are in raw format without any geometric corrections. The leader file of the image data, which contains position and attitude information of satellite during the pass of several scenes, is also available for use. However, the attitude data could not be utilised in this study because the file format was not accessible.

Digitised 1:20000 topographic map and digital elevation model (Korkeusmalli25) were used to acquire ground control. Estimated accuracy of the ground control is ±5 m for X and Y, and ±4 m for Z. Image observations were carried out manually by using Erdas Imagine software. Measured points were divided into two groups: one group used as control points and other as check points, see Fig. 5.

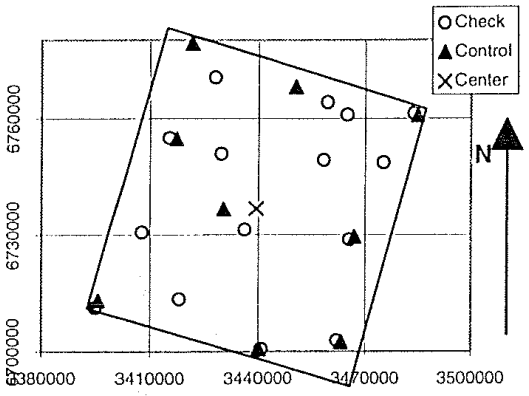

Figure 5a. Distribution of GCPs and check points for the stereo image case.

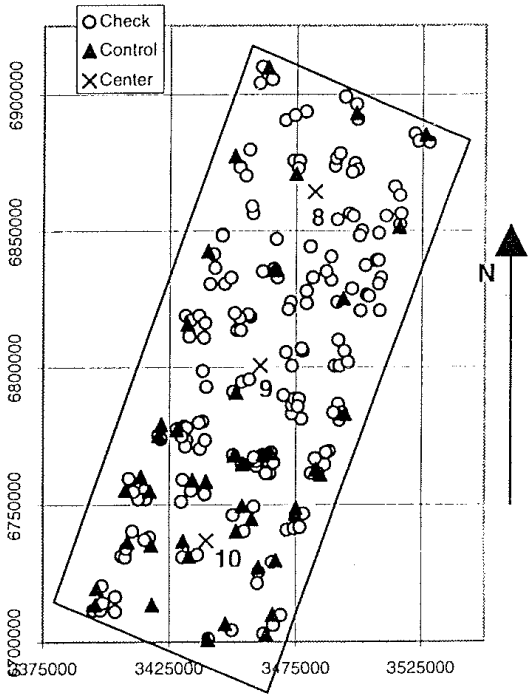

Figure 5b.Distribution of GCPs and check points for three images.

Tie point measurements of stereo image pairs (channel 3 and 4) were performed by automatic tie point measurement system of Finnish Geodetic Institute (FGI). The least squares method is used in the matching.

Approximate values for the orbital parameters were calculated from the ephemeris data. The attitude parameters were set to zero with an exception of the pitch angel for the forward-looking sensor (ρ = 15.33°).

5. TESTS AND RESULTS

The models were tested with following configurations: 1) single image; 2) image strip, and 3) stereo images. In all the cases, accuracy of the orientation with different ground control configurations was evaluated. Distributions of GCPs and check points are shown in Fig. 5. An attitude model with linear term for ρ and constant term for ω and κ was used for all the cases.

5.1 Single image

Three images (8, 9, 10 see Fig. 5b) were adjusted independently by using five sets of control points on each image. The number of control points in the five sets are 4, 6, 9, 18, 30 respectively, and they are as evenly distributed over the images as possible. Fig. 5b shows the configuration of 9 control points for images 8 and 9, and 30 control points for image 10. The evaluation of orientation accuracy was done by transforming the ground coordinates of check points into the image space using the determined orientation parameters. The RMS values of the differences between calculated image coordinates and measured values were computed. The results are shown in Fig. 6 where X is in the direction perpendicular to the CCD array and Y is in the direction of the CCD array.

In general, accuracy of about 0.4 pixels is obtained in X and Y when nine control points were used. Further increase in control points does not improve accuracy significantly.

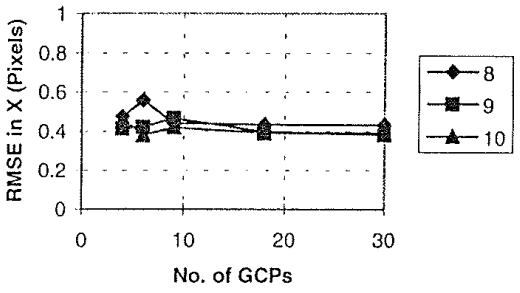

Figure 6a. RMSE in X for single image case.

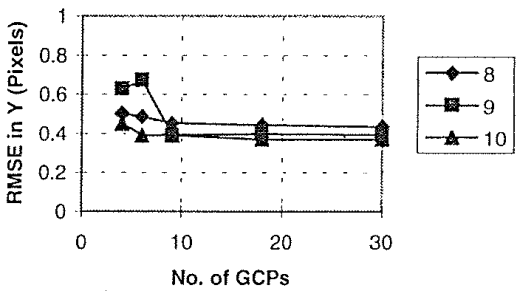

Figure 6b. RMSE in Y for single image case.

5.2 Image strip

A strip of three images were adjusted simultaneously in the block adjustment by using the same number and configuration of ground control points on each image as in single image cases. The results are given in Fig. 7. The expectation from this is that the accuracy should be the same as or better than that in the single image case. This is true when nine or more control points were used. However, the accuracy is worse in Y for images 8 and 10 and in X for image 9 when four or six control points was used. This is probably due to the poor geometry of image 9 (missing lines) which becomes apparent in strip processing.

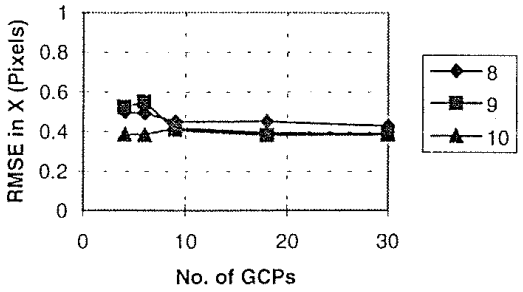

Figure 7a. RMSE in X for image strip case.

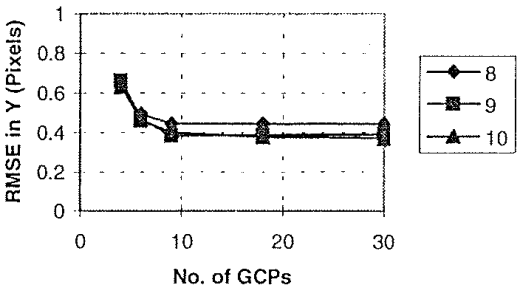

Figure 7b. RMSE in Y for image strip case.

5.3 Stereo measurements

Stereo measurement accuracy were evaluated using the nadir and forward looking channels of the southermost image (10). Tie points were measured automatically. 22 points were measured manually on both channels for controlling and checking. The adjustments were performed with 4, 6, and 9 control points respectively. The rest of the points were served as check points and they were treated as tie points in the adjustments. Fig. 5a shows the configuration of 9 control points. The evaluation of the orientation accuracy was done by comparing the adjusted check point coordinates to the reference values and computing RMS values of the differences. The results are shown in Table 1.

As can be seen from Table 1, amount of control points does not seem to have much influence on the accuracy.

Table 1. RMSE of check points.

		RMSE(m)		
No of GCPs	No. of check points	X	Y	Z
4	18	10.68	7.22	17.89
6	16	9.96	7.24	18.52
9	13	10.39	7.04	18.67

6. CONCLUSIONS AND OUTLOOK

A method for orientation of JERS VNIR images has been implemented into the multisensor aerial triangulation system of Finnish Geodetic Institute. The method can be generalised also to other satellite sensors with CCD linear array geometry.

Empirical tests were performed with three JERS VNIR images. A significant problem was the lack of attitude data which is of great importance for the stability of strip triangulation. In general, RMSEs reduce with increasing amount of control points. With nine ground control points, the planimetric accuracy of about 9.6 m and 7.2 m for X and Y respectively were achieved, corresponding to 0.4 of pixel size. Further increase in control points does not improve accuracy significantly. Accuracy of stereo measurements was 10.68m, 7.22m, 17.89m, for X, Y and Z when four control points were used. The amount of control points does not seem to have much influence on the accuracy for stereo measurements. These results are not as good as those of Westin (Westin 1996), but can be considered satisfactory when taking the missing attitude information into account. Furthermore, measurement errors of the control and check points also have effects on the accuracy.

Presented above are only preliminary results. Investigation of orientation of satellite images will continue at Finnish Geodetic Institute. The multisensor aerial triangulation system will be extended to handle different sensors with pushbroom geometry, first SPOT/HRV and IRS/PAN. Also empirical investigations will be carried out.

7. ACKNOWLEDGEMENTS

This investigation has been financially supported by the Technology Development Centre of Finland and the Finnish mapping companies FM-Kartta Ltd, Geodata Ltd and Mittaustekniikka Ltd. They are gratefully acknowledged.

REFERENCES

Ebner, H., Kornus, W. and Ohlhof, T., 1992. A Simulation Study on Point Determination for the MOMS-02/D2 Space Project Using an Extended Functional Model. International Archives of Photogrammetry and Remote Sensing. Vol. XXIX, Part B4, pp. 458-464.

Jacobsen, K., 1997. Calibration of IRS-1C Pan-camera. ISPRS Joint Workshop "Sensors and Mapping From Space" of Working Groups I/1, I/3 and IV/4, University of Hannover, Germany. pp163-170.

Kratky, V., 1988. Rigorous Photogrammetric Processing of SPOT Images at CCM Canada. ISPRS Journal of Photogrammetry and Remote Sensing, 44. pp. 53-71.

Kratky, V., 1989. On-line Aspects of Stereophotogrammetric Processing of SPOT Images. Photogrammetric Engineering and Remote Sensing, Vol. 55, No. 3, pp. 311-316.

Maruyama, H., Kojiroi, R., Ohtsuka, T., Shimoyama, Y., Hara, S., and Masaharu, H., 1994. Three Dimensional Measurement by JERS-1, OPS Stereo Data. International Archives of Photogrammetry and Remote Sensing. Vol. 30, Part 4, pp. 210-215.

Mikahil, E. M., 1976. Observations and Least Squares. IEP 1976. New York, N.Y.

Nwosu, A., G. and Meid, A., 1996. The Leica System for Orientation of Linear Array Sensor Imagery. International Archives of Photogrammetry and Remote Sensing. Vol. XXXI, Part B3, pp. 585-590.

Neto, F.A., 1992. A model for the Orientation of Along-Track Satellite Stereopairs. International Archives of Photogrammetry and Remote Sensing. Vol. XXIX, Part B4, pp. 315-320.

Priebbenow, R., 1992. Triangulation of SPOT Imagery at the Department of Lands, Queensland. In: Dowman, I.J.,(Ed.). OEEPE Test of Triangulation of SPOT Data.

Westin, T., 1990. Precision Rectification of SPOT Imagery. Photogrammetric Engineering and Remote Sensing, Vol. 56, No. 2, pp. 247-253.

Westin, T., 1991. Pass Processing and Extrapolation of SPOT Image Geometry. Photogrammtric Record, 13(78), pp. 923-929.

Westin T., 1996. Photogrammetric Potential of JERS-1 OPS. International Archives of Photogrammetry and Remote Sensing. Vol. XXXI, Part B4, pp. 937-942.